Cascades of spinodal decompositions in the ternary Cahn-Hilliard equations

David J. Eyre
Department of Mathematics
University of Utah
Salt Lake City, UT 84112
eyre@math.utah.edu

Abstract

The dynamics of the Cahn-Hilliard equations for a ternary alloy are studied during the phase separation process. The results show a primary spinodal decomposition followed by coarsening and then possibly a secondary spinodal decomposition.

1 Introduction.

In this paper, the Cahn-Hilliard (CH) equations for a ternary alloy will be used to study a sequence of spinodal decompositions. The equations model a ternary alloy quenched into a three phase region of the phase diagram.

In the numerical results presented below, it is observed that the solution of the CH equations, under mild restrictions, undergoes a primary spinodal decomposition and becomes a nearly binary material. This pseudo-binary then coarsens and may undergo an additional phase separation. This sequence of spinodal decompositions will be referred to as a cascade.

It is the goal of this paper to present results from numerical simulations that may be of interest to materials scientists, and to provide an intuitive understanding of the resulting observations rather than a rigorous analysis of them.

In the next section, the equations and the initial value problem for spinodal decomposition are given. Then the numerical simulations are presented in §3. A brief review of the primary spinodal decomposition is given in §4. Then the pseudo-binary solutions are studied in §5, and the secondary separation and coarsening processes are studied in §6 and §7.

2 The Cahn-Hilliard Equations.

Consider a ternary alloy held in a closed vessel Ω. Let $u_i(\vec{x},t)$ for $i = 1, 2, 3,$ represent the mole fraction of the components of the alloy as a function of space and time, then by mass conservation and positivity

$$\sum u_i(\vec{x},t) = 1, \quad u_i(\vec{x},t) \geq 0. \tag{1}$$

This restriction implies that (u_1, u_2, u_3) lies on a triangular region of the first orthant known as the Gibbs Triangle, which will be denoted by $\mathcal{G}$.

The Cahn-Hilliard energy functional [2] for this material is

$$\mathcal{F}(u_1,u_2,u_3) = \int_\Omega \left[\Phi(u_1,u_2,u_3) + \frac{\varepsilon^2}{2} \sum_i |\nabla u_i|^2 \right] d\vec{x}. \tag{2}$$

The function $\Phi(u_1, u_2, u_3)$ is the Gibbs free energy per unit volume, ε is the gradient energy coefficient, and ∇ is the spatial gradient operator. The average composition of the alloy is conserved because the alloy is held in a closed vessel, so

$$\frac{1}{|\Omega|} \int_\Omega u_i(\vec{x}) d\vec{x} = \bar{u}_i \quad \text{for } i = 1, 2, 3. \tag{3}$$

The alloy being modeled is assumed to be a regular solution [12], so the Gibbs free energy will have the form

$$\Phi(u_1,u_2,u_3) = \sigma \sum_{i \neq j} u_i u_j + \sum_{i=1}^{3} u_i \log u_i, \tag{4}$$

where σ is inversely proportional to temperature. If $\sigma \geq 3$, then $\Phi(u_1, u_2, u_3)$ has three minima and one local maximum in $\mathcal{G}$. This energy allows for one, two and three phase materials, along with spinodal and metastable regions of $\mathcal{G}$.

The dynamic CH equations are derived from (1)-(3) and can be represented as

$$\frac{\partial}{\partial t}\mathbf{u} = \Delta\left[-\varepsilon^2\Delta\mathbf{u} + \mathbf{f}(\mathbf{u})\right] \tag{5}$$

where

$$\mathbf{u} \stackrel{\text{def}}{=} (u_1, u_2), \quad u_3 = 1 - u_1 - u_2, \quad \vec{x} \in \Omega, \quad t > 0. \tag{6}$$

The nonlinear function $\mathbf{f}(\mathbf{u})$ is

$$\mathbf{f}(\mathbf{u}) = P\nabla_u\Phi(u_1, u_2, u_3)|_{u_3=1-u_1-u_2} \tag{7}$$

where P is appropriate projector from $\mathbf{R}^3$ into the span of all vectors containing $\mathcal{G}$. The operator Δ is the Laplacian. As in the binary case, $\mathcal{F}(u_1, u_2, u_3)$ is a nonincreasing energy functional of the dynamic equations.

The natural and average conserving boundary conditions for the system are

$$\nabla\mathbf{u}\cdot\vec{n}\,|_{\vec{x}\in\partial\Omega} = \nabla(\Delta\mathbf{u})\cdot\vec{n}\,|_{\vec{x}\in\partial\Omega} = \mathbf{0}. \tag{8}$$

respectively. The simulations presented in this paper will employ periodic boundary conditions. These boundary conditions also leave $\bar{\mathbf{u}}$ invariant in time.

The initial conditions used in this paper will model the nearly homogeneous prequenched material as

$$\mathbf{u}(\vec{x}, 0) = \bar{\mathbf{u}} + \tilde{\mathbf{u}}(\vec{x}), \quad |\tilde{\mathbf{u}}(\vec{x})|_\infty \ll 1, \tag{9}$$

where $\tilde{\mathbf{u}}(\vec{x})$ is a zero average, small perturbation of $\bar{\mathbf{u}}$.

Mathematical issues related to the Cahn-Hilliard equation have been reviewed recently by Elliott [4]. Generalization of the CH equations to multicomponent systems appears first with deFontaine [3], and with Morral and Cahn [11]. Subsequently the studies reappear recently in the metallurgical literature with Hoyt [10]. Mathematical results include the existence and uniqueness theory of Elliott and Luckhaus [5] and a survey by Eyre [6].

In particular, Elliott and Luckhaus [5] proved the well-posedness of the equations, and proved that the solution remains within $\mathcal{G}$ for all time, i.e. that each component remains positive.

3 Cascades of Spinodal Decomposition.

Numerical simulations are now given that show the spinodal decomposition processes of the ternary solution.

In the simulations, the average composition of the first two metals are equal and the average composition of the third metal is varied. The precise average for each simulation is given below. The parameters in the model were chosen to be

$$\sigma = 3.5, \quad \varepsilon^2 = 5\times10^{-4} \tag{10}$$

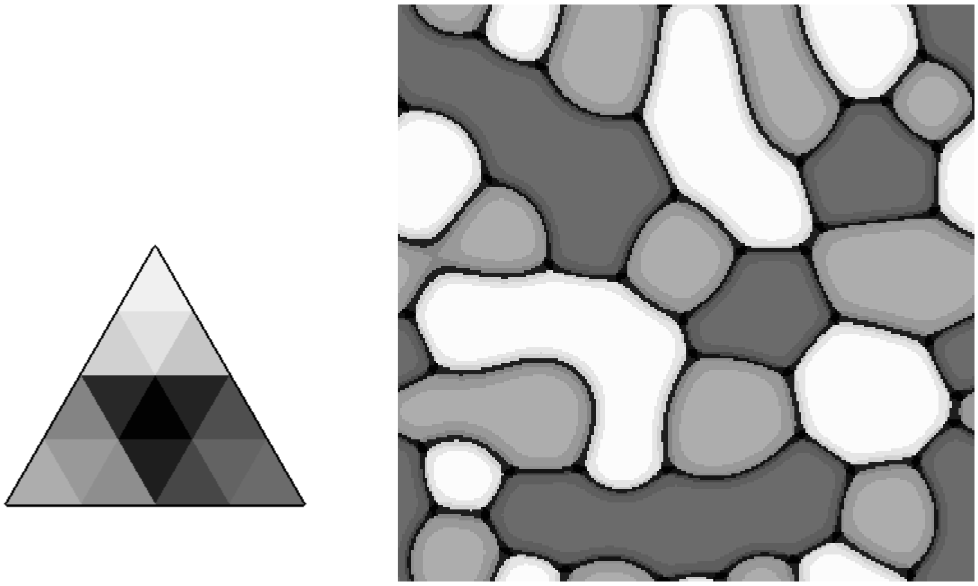

Figure 1: Gray scale representation of the Gibbs triangle and the spatial features of a solution.

and periodic boundary conditions were employed. In all the simulations presented the initial data (9) was random, generated uniformly on $(\bar{\mathbf{u}} - 0.01, \bar{\mathbf{u}} + 0.01)$.

The simulations are presented as time snapshots using a gray scale representation of $\mathbf{u}$ by mapping $\mathbf{u}$ to the shaded Gibbs triangle shown in Figure 1. Specifically, $\mathcal{G}$ was subdivided into 16 equal area triangles, and each subtriangle given a unique shade. Furthermore, notice that $\mathcal{G}$ in Figure 1 can be coarsely divided into four subtriangles where the top triangles are the lightest, the lower left triangles are dark, the lower right triangles are darker still, and central triangles are the darkest.

Figure 1 also presents a snapshot of the solution of the CH equations. The solution is shown in the physical domain on a 256^2 grid. The most striking feature of the solution is that it appears to be roughly piecewise-constant over large regions of space, defining three distinct phases. The three phases indicate the solution takes values near each vertex in $\mathcal{G}$ over large regions of space.

Between the distinct phases the solution has a graduated shading that represents the interfaces. Notice that the width of the interfaces is measurable and that the interfaces are diffuse. The solution in the interface can be estimated by comparing the interface shading with the gray scale map.

In Figures 2, 3, and 4 below, three different simulations are presented, and six snapshots are given for each simulation. Time increases across the rows and down the columns, so the earliest snapshot is on the top left and the latest snapshot is on the bottom right. The exact times for each simulation are given below, but in every case the snapshots are equally spaced on a logarithmic time scale. The first frame in every case shows the spinodally decomposed pseudo-binary solution. This solution has already evolved from the nearly constant initial conditions.

In all the simulations presented below, equilibrium theory given in [6] predicts that the lowest energy state of the material will have three phases.

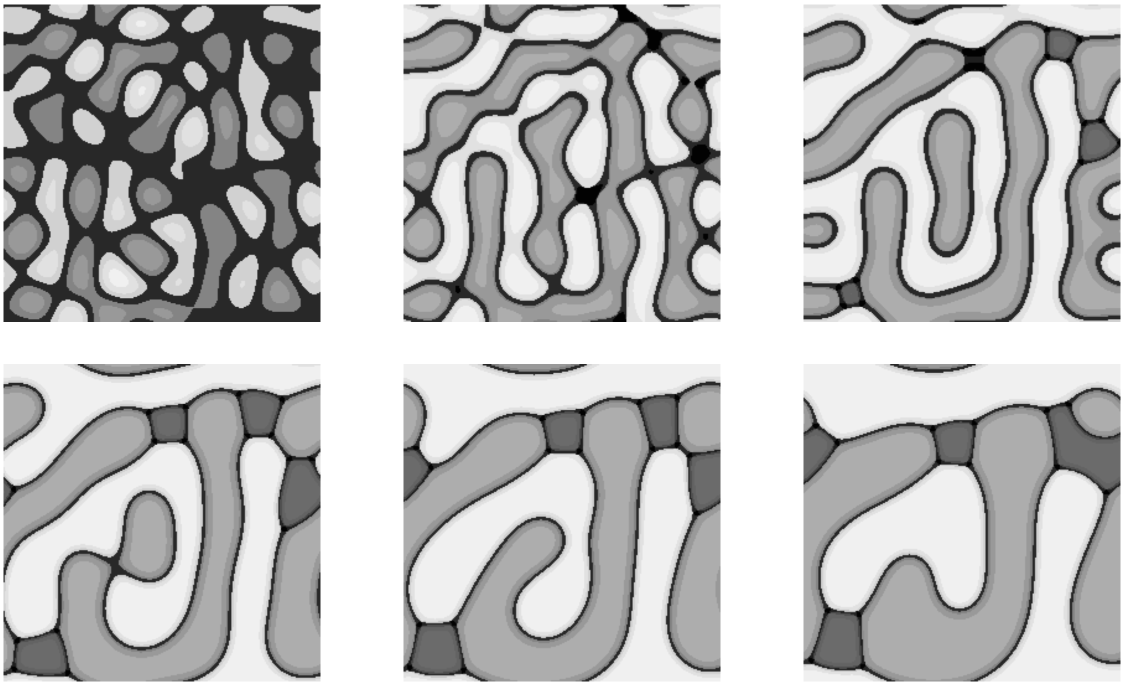

Figure 2: Three phase separation with $\bar{\mathbf{u}} = (0.43, 0.43)$.

The average composition of the simulation presented in Figure 2 is $\bar{\mathbf{u}} = (0.43, 0.43)$. The time of the earliest snapshot is $t_1 = 0.001$ and $t_{j+1} = 2.154\, t_j$. The early stages of the evolution are marked by the finest scale perturbations of $\mathbf{u}(x, 0)$ smoothing rapidly followed by separation into a two phase material or a pseudo-binary. The pseudo-binary solution undergoes coarsening and then phase separates a distinct third phase. The third phase appears in the interfacial regions.

In Figure 3, the average composition of the solution is $\bar{\mathbf{u}} = (0.25, 0.25)$. The time of the earliest snapshot is $t_1 = 0.001$ and $t_{j+1} = 1.778\, t_j$. This simulation also shows a detailed pseudo-binary phase separation, followed by pattern coarsening, and finally a secondary phase separation.

The secondary phase separation processes shown in Figure 2 and 4 are quite different. Notice that in Figure 3, the primary separation leaves two distinct phases, and then in the secondary separation, one of those phases decomposes into two different phases. In the end, one phase of the pseudo-binary observed after primary separation is gone.

In Figure 2, during secondary separation, small inclusions of the third phase appear in regions where there was an interface between the phases of the pseudo-binary. In the end, both of the phases of the pseudo-binary are still present.

In Figure 4, the average composition of the solution is $\bar{\mathbf{u}} = (0.46, 0.46)$. The time of the earliest snapshot is $t_1 = 0.001$ and $t_{j+1} = 1.778\, t_j$. This simulation also shows a detailed pseudo-binary phase separation, followed by pattern coarsening, but this solution does not undergo secondary phase separation.

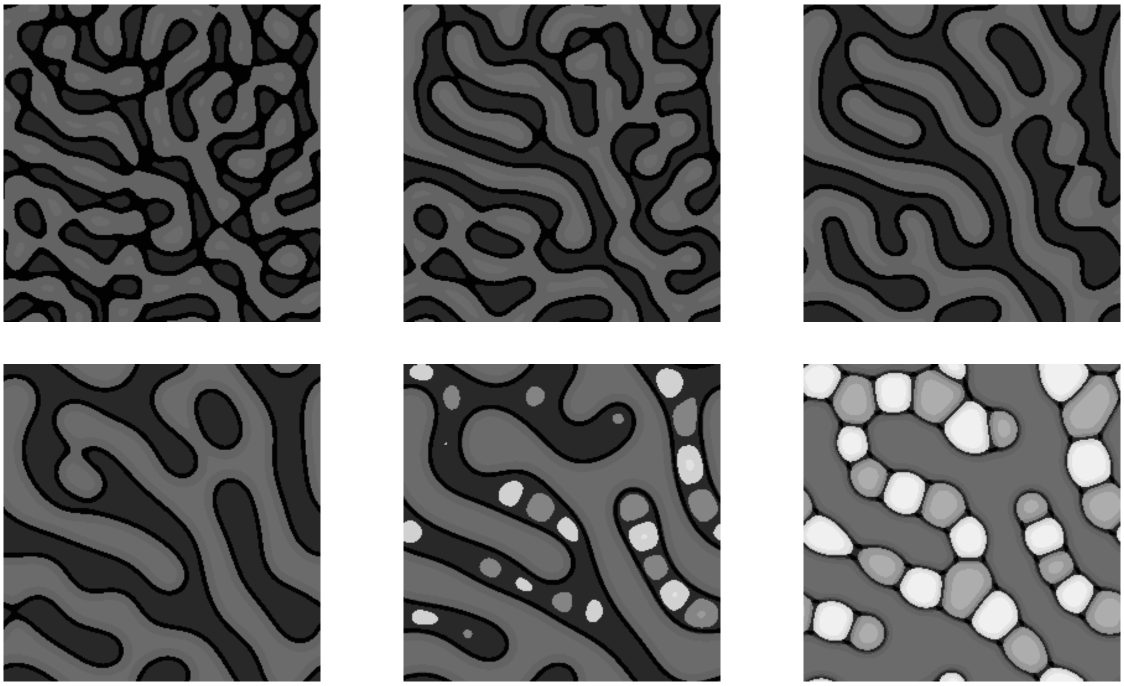

Figure 3: Three phase separation with $\bar{\mathbf{u}} = (0.25, 0.25)$.

4 Primary spinodal decomposition.

In this section, the transition from a nearly constant solution to a pseudo-binary solution is reviewed. This analysis is due to Morral and Cahn [11].

It can be easily seen that any constant value $\bar{\mathbf{u}}$ is a stationary solution of (5), and a natural question to consider is the stability of the average. For simplicity, the stability analysis will be carried out on $\Omega = [0, \ell_1] \times [0, \ell_2]$. In this case, the linearized CH equation is

$$\mathbf{u}_t = -\Delta \left[\varepsilon^2 \Delta \mathbf{u} - D(\bar{\mathbf{u}})\mathbf{u} \right] \tag{11}$$

where D is the Jacobian of $\mathbf{f}$. If n_1 and n_2 are integers, then by separation of variables, (11) admits a solution of the form

$$\mathbf{u}(\vec{x}, t) = \sum_k \tilde{\mathbf{v}}_k(t) \sum_{n_1, n_2 \in \mathcal{A}} \cos \frac{n_1 \pi x_1}{\ell_1} \cos \frac{n_2 \pi x_2}{\ell_2} \tag{12}$$

where the index set of the second sum is

$$A = \left\{ n_1,\ n_2 \middle| \pi \sqrt{\frac{n_1^2}{\ell_1^2} + \frac{n_2^2}{\ell_2^2}} = k \right\}.$$

Since the terms of the summation are orthogonal with respect to the standard L^2 inner product, each term of the sum must satisfy the equation. A short calculation of the derivatives yields the following differential equation for $\tilde{\mathbf{v}}_k(t)$,

$$\frac{d\tilde{\mathbf{v}}_k(t)}{dt} = -k^2 \left(k^2 \varepsilon^2 I + D \right) \tilde{\mathbf{v}}_k(t). \tag{13}$$

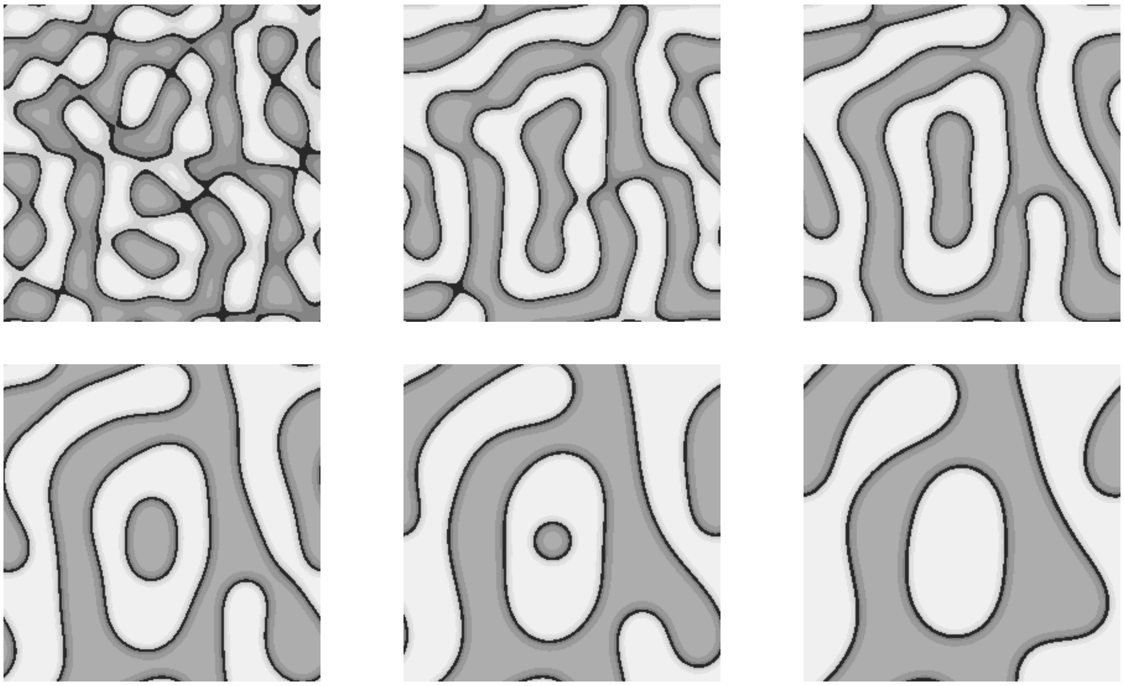

Figure 4: Metastable binary intermediate with $\bar{\mathbf{u}} = (0.46, 0.46)$.

To express the solution of (13) analytically, let ξ_1 and ξ_2 be the eigenvalues of D, and let $\mathbf{v}_1$ and $\mathbf{v}_2$ be the corresponding eigenvectors, then the eigenvalues and eigenvectors of the ode (13) satisfy

$$-k^2(k^2\varepsilon^2 I + D)\mathbf{v}_i = \left[-k^2(k^2\varepsilon^2 + \xi_i)\right]\mathbf{v}_i. \tag{14}$$

By denoting $\lambda_i(k) = -k^2(k^2\varepsilon^2 + \xi_i)$, the solution of the linear odes for $\tilde{\mathbf{v}}_k(t)$ are

$$\tilde{\mathbf{v}}_k(t) = c_k e^{\lambda_1(k)t}\mathbf{v}_1 + d_k e^{\lambda_2(k)t}\mathbf{v}_2 \tag{15}$$

where c_k and d_k are determined from the initial conditions. This solution can be easily studied as a function of k and D.

As a function of k, there are two interesting cases. First notice that for large k, $d\tilde{\mathbf{v}}_k/dt$ is dominated by $-\varepsilon^2 k^4$, therefore, in this case $\tilde{\mathbf{v}}_k \to \mathbf{0}$. This occurs if the wavenumbers n_i is sufficiently large or if the domain sizes ℓ_i are sufficiently small. Furthermore, in a closed domain, the eigenvalues of (11) are discrete, so for small enough ℓ_i, all the eigenvalues are negative and $\tilde{\mathbf{v}}_k \to \mathbf{0}$.

For small k, $d\tilde{\mathbf{v}}_k/dt$ is dominated by the eigenvalues of D, and there are three interesting cases:

- If D is positive definite, then $\xi_1, \xi_2 > 0$, and every $\lambda_i(k) < 0$. Consequently $\bar{\mathbf{u}}$ is locally stable with respect to small perturbations. This case occurs where Φ is convex, i.e. in the stable one-phase region of $\mathcal{G}$, in the classical metastable regions of $\mathcal{G}$ and in all of $\mathcal{G}$ at high temperatures.

- If D is indefinite, then $\xi_i < 0 < \xi_2$, and $\lambda_i(k) > 0 > \lambda_j(k)$ when $k < k_c$. Consequently, $\bar{\mathbf{u}}$ is unstable with respect to generic perturbations in the direction

$\mathbf{v}_i$ and $\bar{\mathbf{u}}$ is stable with respect to all perturbations in the $\mathbf{v}_j$ direction. For short-times, the solution can be written as a perturbation of the average in the direction of $\mathbf{v}_i$ as

$$\mathbf{u}(\vec{x},t) = \bar{\mathbf{u}} + \Theta(\vec{x},t)\mathbf{v}_i \tag{16}$$

where $\Theta(\vec{x},t)$ is the superposition of all the fourier modes corresponding to the direction $\mathbf{v}_i$. This case occurs where $\bar{\mathbf{u}}$ is in a subset of the spinodal region of $\mathcal{G}$.

- If D is negative definite, then $\xi_1, \xi_2 < 0$, and $\lambda_2(k), \lambda_2(k) > 0$ when $k < k_c$. Consequently, $\bar{\mathbf{u}}$ is unstable with respect to all generic initial conditions in the span of $\mathbf{v}_1$ and $\mathbf{v}_2$. This case also occurs where $\bar{\mathbf{u}}$ is in a subset of the spinodal region of $\mathcal{G}$.

An important result of [11] is that if the solution separates, then it will separate into a pseudo-binary because generically the linearized equations will have a unique largest growth mode, and that mode will dominate.

5 Pseudo-binary solutions on lines.

In this section, the pseudo-binary (16) is examined. It will be assumed that $\bar{\mathbf{u}}$ is in the spinodal region, and that $\mathbf{v}_1$ is the direction of fastest separation.

The ternary Cahn-Hilliard equation can be projected onto $\mathbf{v}_1$ to give a binary Cahn-Hilliard equation for $\Theta(\vec{x},t)$

$$\Theta_t = -\Delta\left[\varepsilon^2\Delta\Theta - f(\Theta)\right] \tag{17}$$

where $f(\Theta) = \langle \mathbf{f}(\bar{\mathbf{u}} + \Theta\mathbf{v}_1), \mathbf{v}_1\rangle$. This equation is found by substituting (16) into (5) and taking the dot product of the resulting equation with $\mathbf{v}_1$. The solution of (17) will not generically be a solution of (5), but it is interesting to study. Furthermore, Figure 5 shows that (5) it is a reasonable representation of the solutions presented in Figures 2 and 3. In Figure 5, the solution $\mathbf{u}(\vec{x},t)$ is mapped onto $\mathcal{G}$. The solution for the simulation in Figure 2 lies on a curve while the solution for the simulation in Figure 3 lies on a line.

By construction, the mass of (16) is $\bar{\mathbf{u}}$ if $\bar{\Theta} = 0$. However, there exist families of $\bar{\mathbf{u}} \in \mathcal{G}$ that have identical eigenvectors and the pseudo-binaries lie on identical subsets of $\mathcal{G}$, so to study the effects of $\bar{\mathbf{u}}$ on the solutions of this form, a different average can be selected from this family. An example of this is shown in Figure 6 where the pseudo-binary for three different average compositions that each satisfy (16) for different Θ's are shown. The relative fractions of the separated phases change between simulations because the position of $\bar{\mathbf{u}}$ relative to the unstable zero of $f(\Theta)$ is changing.

The nonlinearity $f(\Theta)$ is the directional derivative $\partial\Phi/\partial P^T\mathbf{v}_1$ since $\mathbf{f}(\mathbf{u})$ is given by (7), and

$$f(\Theta) = \langle P\nabla_u\Phi(u_1,u_2,u_3), \mathbf{v}_1\rangle = \left\langle \nabla_u\Phi(u_1,u_2,u_3), P^T\mathbf{v}_1\right\rangle. \tag{18}$$

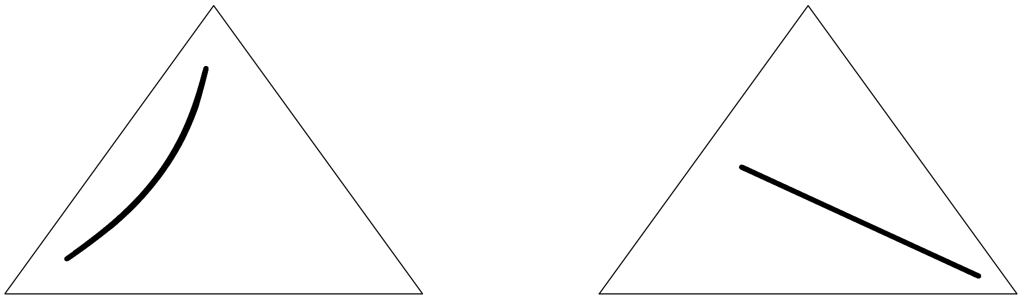

Figure 5: Pseudo-binary solutions of the CH equations with average compositions (0.43,0.43) and (0.25,0.25) mapped into $\mathcal{G}$.

Furthermore, since it has been assumed that $\bar{\mathbf{u}}$ is in the spinodal and $\mathbf{v}_1$ is the direction of fastest separation, then it must be that $f(\Theta)$ is a bistable type nonlinearity. So it is expected that Θ will vary between the stable zeros of $f(\Theta)$. If Θ_1^* and Θ_2^* are the stable zeros of $f(\Theta)$, then

$$\mathbf{u}_i = \bar{\mathbf{u}} + \Theta_i^* \mathbf{v}_1 \tag{19}$$

are the locations of the stable zeros within $\mathcal{G}$, and the values of (16) will take values in $\mathcal{G}$ between $\mathbf{u}_1$ and $\mathbf{u}_2$.

It is also interesting to consider the properties of the pseudo-binary solution as a function of $\mathbf{u}_1$ and $\mathbf{u}_2$. There are three interesting distinct possibilities for these locations; Both of the zeros may be in the spinodal region of $\mathcal{G}$, both of the zeros may be in a stable (or metastable) region of $\mathcal{G}$, or one zero may be in the spinodal region and the other in the stable region.

The numerical simulations presented above provide examples of these possibilities. The pseudo-binary presented in Figure 2 is an example of spinodal-spinodal pair, i.e. the zeros of $f(\Theta)$ are in the spinodal region of $\mathcal{G}$.

The pseudo-binary presented in Figure 3 is an example of spinodal-stable pair, i.e. one stable zero of $f(\Theta)$ is in a stable region of $\mathcal{G}$ and the other is in the spinodal region of $\mathcal{G}$.

The pseudo-binary presented in Figure 4 is an example of stable-stable pair, i.e. the zeros of $f(\Theta)$ are in the stable region of $\mathcal{G}$.

As mentioned above, this representation of the pseudo-binary is not generically a solution of (5), but in a forthcoming paper [7], a pseudo-binary that is a solution (5) for any $\bar{\mathbf{u}}$ will be given and studied.

6 Predicting secondary separation.

If the pseudo-binary (16) is not too far from the solution of (5), then predicting and understanding the secondary separation process is equivalent to studying the stability of (16) with respect to perturbations in the direction of $\mathbf{v}_2$.

Given the observations of the previous section, it should not be surprising that secondary separation occurs in the first two simulations. To understand why, consider

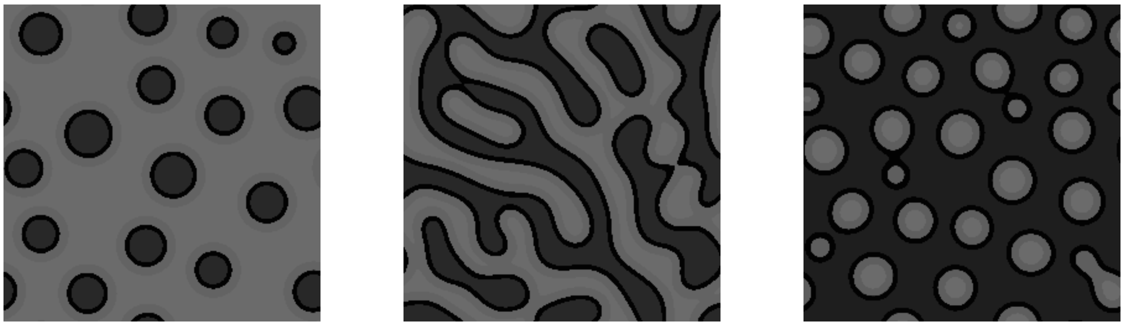

Figure 6: Different average compositions of the pseudo-binary.

a homogeneous solution $\mathbf{u} = \mathbf{u}_i$ given in (19). If $\mathbf{u}_i$ is in a spinodal region of $\mathcal{G}$, this solution is generically unstable. The direction of maximal instability is uncertain, but the direction orthogonal to $\mathbf{v}_1$ is unstable.

Now consider the implications of this on (16) and (17). The solution of (17) will be near the zeros of $f(\Theta)$ except in the interfaces between phases. Therefore, much of the pseudo-binary will be near $\mathbf{u}_i$ and consequently, within the spinodal region of $\mathcal{G}$. So it seems reasonable to believe that the pseudo-binary is unstable.

On the other hand, if $\mathbf{u} = \mathbf{u}_i$ is in a stable or metastable region of $\mathcal{G}$, then much of the pseudo-binary will be within a locally stable region of $\mathcal{G}$, and consequently the pseudo-binary should be locally stable.

These observations are seen in the numerical simulations. In Figure 4, the pseudo-binary has both zeros of $f(\Theta)$ near minima of Φ. Consequently, the solution is locally stable and does not undergo secondary separation. It is worth stressing however, that the global energy minimizer for this solution has three phases, and therefore this pseudo-binary is metastable.

In Figure 3, the pseudo-binary has one zero of $f(\Theta)$ near a saddle point of Φ while the other zero is near a minimum of Φ. The saddle is unstable with respect to separation into two additional phases, therefore the material in one of the tube-like spatial structures is near this saddle, and decomposes into two distinct phases. The phase within the other tube-like structure is near the minimum and appears unchanged after secondary separation.

In Figure 2, both stable zeros of $f(\Theta)$ are in a spinodal region of $\mathcal{G}$ and consequently a third phase appears. The obvious question that remains is why this secondary separation results in an inclusion-type geometry. This is fairly easy to understand. In this case, primary decomposition does give pseudo-binary, but not of the form (16). The true pseudo-binary lies on a curve in $\mathcal{G}$ as opposed to a straight line. The endpoints of this curve are near the minima of Φ, and consequently the interface between these minima is curved towards the centroid of $\mathcal{G}$ to balance the mass of the solution. As the interface becomes more curved it eventually enters the spinodal region of $\mathcal{G}$ that is unstable with respect to separation in the third phase. At this point there is no longer an activation like energy barrier to creating the third phase, and the solution can lower its free energy by fully separating. Consequently, the third phase appears within the interface itself. A detailed analysis of this process will be included in [7].

7 Coarsening of the pseudo-binary.

In this final section, the coarsening between primary and secondary separation is examined and a geometric argument is given to justify the observations made from the simulations given in Figures 3 and 4. A detailed mathematical description of this process has been completed and will appear in [7].

To understand the coarsening phenomena, it is useful to recall the following two concepts. First, it is known that immediately after spinodal decomposition, solutions of the binary Cahn-Hilliard equation are highly oscillatory, nearly periodic and the separation length between like phases is $O(\varepsilon)$ [1, 9]. Pseudo-binary solutions of the ternary alloy CH equations are very similar to solutions of the binary CH equation, and so it is reasonable to expect that that they too will be highly oscillatory and nearly periodic. The simulations presented in Figures 3, 4 and 5 confirm this expectation.

Second, it was shown in §5, that if the domain size in either direction was small, spinodal decomposition can be inhibited because the eigenvalues of the spatial operator are discrete.

Now the simulation given in Figure 2 will be used to give an intuitive argument for the coarsening. The pseudo-binary in this case has one stable phase and one unstable phase. Both phases are highly oscillatory and occupy narrow tube-like regions of space, and the unstable phase does not decompose until the width of the tubes has increased significantly.

If these observations are considered in light of the concepts just discussed, the immediate conclusion that can be drawn is that the initial domain size of the spinodally decomposed pseudo-binary is so small that it inhibits secondary separation. Thus the unstable phase of the pseudo-binary has an effective domain, in this case the tubes, and the effective domain must be sufficiently large for secondary separation to take place.

Acknowledgments

This work was partially supported by an ARO contract with the University of Minnesota's AHPCRC.

References

[1] J. W. Cahn, *On spinodal decomposition*, Acta Metallurgica, 9 (1961), pp. 795–801.

[2] J. W. Cahn and J. E. Hilliard, *Free energy of a nonuniform system - I. Interfacial free energy*, J. Chem. Phys., 28 (1958), pp. 258-267.

[3] D. DeFontaine, Ph.D. Thesis, Northwestern University, 1967.

[4] C. M. ELLIOTT, *The Cahn-Hilliard model for the kinetics of phase separation*, in Mathematical Models for Phase Change Problems, J. F. Rodrigues, ed., Birkhäuser Verlag, Basel, 1989, pp. 35–73.

[5] C. M. ELLIOTT AND S. LUCKHAUS, *A generalised diffusion equation for phase separation of a multi-component mixture with interfacial free energy*, IMA preprint 887.

[6] D. J. EYRE, *Systems of Cahn-Hilliard Equations*, SIAM J. Appl. Math., 53, (1993), pp. 1686-1712.

[7] D. J. EYRE, in preparation.

[8] P. C. FIFE, *Models for phase separation and their mathematics*, in Proceedings, Taniguchi International Symposium on Nonlinear Partial Differential Equations and Applications, Kinokuniya Publishing, 1990.

[9] C. P. GRANT, Ph.D. Thesis, University of Utah, 1991.

[10] J. J. HOYT, *Spinodal decomposition in ternary alloys*, Acta Metall., 37 (1989), pp. 2489-2497.

[11] J. E. MORRAL AND J. W. CAHN, *Spinodal decomposition in ternary systems*, Acta Metall., 19 (1971), pp. 1037-1045.

[12] D. A. PORTER AND K. E. EASTERLING, *Phase Transformations in Metals and Alloys,* Van Nostrand Reinhold (International), London, 1981.